L1 Adaptive Speed Control of a Small Wind Energy Conversion System for Maximum Power Point Tracking

Zhao, Haoran; Wu, Qiuwei; Rasmussen, Claus Nygaard; Blanke, Mogens

Published in:
I E E E Transactions on Energy Conversion

Link to article, DOI:
10.1109/TEC.2014.2312978

Publication date:
2014

Document Version
Early version, also known as pre-print

$\mathcal{L}_1$ Adaptive Speed Control of a Small Wind Energy Conversion System for Maximum Power Point Tracking

Haoran Zhao, Qiuwei Wu, Claus Nygaard Rasmussen and Mogens Blanke

***Abstract*-- This paper presents the design of an $\mathcal{L}_1$ adaptive controller for maximum power point tracking (MPPT) of a small variable speed Wind Energy Conversion System (WECS). The proposed controller generates the optimal torque command for the vector controlled generator side converter (GSC) based on the wind speed estimation. The proposed MPPT control algorithm has a generic structure and can be used for different generator types. In order to verify the efficacy of the proposed $\mathcal{L}_1$ adaptive controller for the MPPT of the WECS, a full converter wind turbine with a squirrel cage induction generator (SCIG) is used to carry out case studies using Matlab/Simulink. The case study results show that the designed $\mathcal{L}_1$ adaptive controller has good tracking performance even with unmodeled dynamics and in the presence of parameter uncertainties and unknown disturbances.**

***Index Terms*-Full-converter wind turbine, $\mathcal{L}_1$ adaptive control, maximum power point tracking (MPPT), wind energy conversion system (WECS).**

I. Introduction

WIND power, as an alternative to fossil fuels, is plentiful, renewable, widely distributed, and produces no greenhouse gas (GHG) emission during operation [1]. By the end of 2010, wind energy covered more than 2.5% of the total worldwide electricity consumption, growing more than 25% per year. In 2011, 83 countries around the world were using wind power on a commercial basis [2].

According to the speed control criterion, Wind Energy Conversion Systems (WECSs) can be classified into two types: fixed speed and variable speed. Due to the regulation of rotor speed within a larger range for better aerodynamic efficiency, the variable speed wind turbines are more widely used. Different wind conditions and control purposes change the control objectives of the variable speed wind turbine. Assuming speed and power capture constraints are respected, the controller aims to limit the wind power captured when the wind speed is larger than the nominal speed and maximize the wind power harvested in the partial load regime.

This paper focuses on the control of wind turbines in the partial load regime which generally aims at maximum power point tracking (MPPT) by adjusting the electrical generator speed [3]. Various MPPT control methods for WECSs have been proposed in the literature. These methods can be classified into three control concepts [4], [5]: hill-climbing search (HCS) control, power signal feedback (PSF) control and tip speed ratio (TSR) control. The HCS control normally requires the rotor speed and the turbine power variation as inputs for the MPPT. Recently, other variables, like the dc-link voltage and the duty cycle, are used as the inputs as well [6], [7]. It has the advantage of using very few parameters and little feedback information as well as being simple and robust [8], [9]. However, it is more feasible to use the HCS control in the slow varying system such as PV systems, and not for WECS with fast wind speed changes [10]. The PSF control based on the maximum power curve of the wind turbine needs the rotor speed for calculating the power reference [11] and the tracking speed is dependent on the rotor inertia of the wind turbine [12]. Larger rotor inertia leads to the slow tracking speed which further affects the efficiency, especially in the low wind speed condition. The TSR control directly regulates the rotational speed to keep the optimal TSR. Compared with the other two control methods, additional wind speed information should be provided for the TSR control. One solution is to use anemometers; however, due to the location constraints, the measurement accuracy is limited [11], [13]. Alternatively, the effective wind speed could be estimated in order to avoid the complexity and the cost of external anemometers [14]. Several wind speed estimation methods have been presented in [15]-[18]. The TSR control concept with wind speed estimation is utilized in this paper for the MPPT of wind turbines.

A number of advanced control techniques have been designed based on the TSR control concept for the MPPT of wind turbines. The Proportional Integration (PI) controller is simple and robust, and has been widely used [19]. It is designed based on a linearized WECS model at a steady-state operating point. However, its dynamic performance is expected to vary with the change of the operating point. The sliding mode controller (SMC) is effective and intrinsically robust, requiring little information and is insensitive to parameter variation [20], [21]. The main drawback of the

H. Zhao and Q. Wu are with Center for Electric Power and Energy, Department of Electrical Engineering, Technical University of Denmark, Kgs. Lyngby, 2800, Denmark, and Sino-Danish Center for Education and Research, Aarhus, 8000 Denmark (email: hzhao@elektro.dtu.dk, qw@elektro.dtu.dk).

C. N. Rasmussen is with Center for Electric Power and Energy, Department of Electrical Engineering, Technical University of Denmark, Kgs. Lyngby, 2800, Denmark (email: cnras@elektro.dtu.dk).

M. Blanke is with the Automation and Control Group at Department of Electrical Engineering, Technical University of Denmark, Lygnby, 2800 Demark (email: mb@elektro.dtu.dk) and with the AMOS Center of Excellence, Institute for Technical Cybernetics, Norwegian University of Science and Technology, 7491 Trondheim, Norway.

SMC controller is the chattering. It might result in unmodeled dynamics and produce destructive oscillations [19]. The feedback linearization is appropriate and effective for nonlinear WECSs [22]. However, its formulation is based on specific system modeling which may not be available. Fuzzy logic controllers proposed in [23], [24] do not require accurate and linear system model. However, the stability of the fuzzy system is difficult to guarantee due to the lack of mathematical descriptions.

Recently, the $\mathcal{L}_1$ adaptive control was developed by Hovakimyan and Cao [25]. Compared with the aforementioned control techniques, it demonstrates several advantages. Firstly, the $\mathcal{L}_1$ adaptive control design does not require the accurate system model. Secondly, it guarantees system stability and robust transient performance with fast adaptation to uncertainties [25]-[27] with design tradeoffs [28] and the comparison with other adaptive techniques is presented in [29]. Considering the non-linearity and uncertainty of WECSs, it is suitable to apply the $\mathcal{L}_1$ adaptive control to design the MPPT controller for WECSs. In this paper, an $\mathcal{L}_1$ adaptive controller has been developed for the MPPT of WECSs.

The paper is organized as follows: Section II describes different parts of the generator control system of WECSs. The design of the TSR $\mathcal{L}_1$ controller is presented in Section III. Case studies with the developed TSR $\mathcal{L}_1$ controller are presented and discussed in Section IV. In the end, the conclusion is drawn.

II. Generator Control System of WECSs

The TSR control structure based on wind speed estimation is shown in Fig. 1. A full converter wind turbine with a SCIG is used to illustrate the generator control system of variable speed WECSs. With the measurement of the generator speed and power, the optimal reference generator speed can be derived and fed to the speed control block. Compared with the measured generator speed, the speed controller generates the torque reference as the input to the torque controller. A vector control is employed for the torque controller to generate the control signals for the grid side converter (GSC). The control blocks are described in detail in the subsections A-C.

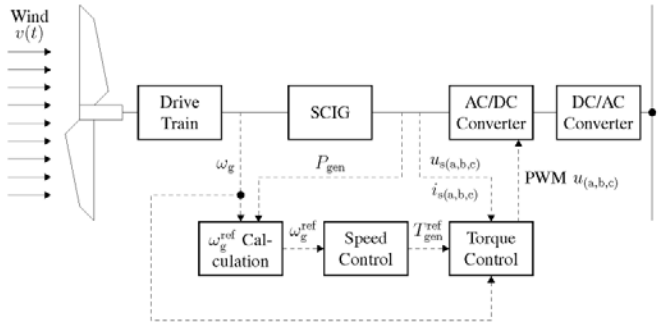

Fig. 1 Generator control of WECSs based on TSR.

A. Optimal Generator Speed Reference Calculation

Block one calculates the optimal generator speed reference ω_g^{ref}. The power balance estimator, widely applied in the wind turbine industry [18], is adopted in this paper .

The power coefficient C_p represents the power extraction efficiency of a wind turbine. It is a function of the tip speed ratio λ and the pitch angle β in a pitch-controlled wind turbine. During the partial load operation, the pitch control system is typically inactive: $\beta = 0$ [30]. The C_p is simplified and represented as a polynomial in λ and the power extraction by the wind turbine can be expressed as,

$$P_{wt} = \frac{1}{2}\cdot\rho\pi R^2 v^3 C_p(\lambda) = \frac{1}{2}\cdot\frac{C_p(\lambda)}{\lambda^3}\rho\pi R^5\omega_r^3, \lambda = \frac{\omega_r R}{v} \quad (1)$$

where ρ is the air density, R is the blade length, v is the wind speed, ω_r is the rotor speed. There is an optimal tip speed ratio λ_{opt} with the maximum C_p^{max}. In order to have the system operating at λ_{opt}, ω_g^{ref} can be obtained as,

$$\omega_g^{ref} = i\frac{\lambda_{opt} v}{R}, \quad (2)$$

where i is the gear ratio. It is noted that λ_{opt} and C_p^{max} are derived by the simplified expression of C_p and assumed to be fixed. However, the polynomial coefficients are time-varying during the actual operation. This will affect the calculated reference ω_g^{ref} and the dynamic performance of the controller.

Instead of using anemometers, the effective wind speed over the rotor is estimated in this study. An estimator is employed to estimate a smoothed version of aerodynamic torque $\hat{T}_a$ and the rotor speed $\hat{\omega}_r$. If the drive train was infinitely stiff, $\hat{T}_a$ can be calcualted by,

$$\hat{T}_a(s) = \frac{1}{1+s\tau}(J_{eq}\, s\,\hat{\omega}_r(s) + T_g(s) + T_{loss}(s)) \quad (3)$$

where J_{eq} is the equivalent inertia of the drive train: $J_{eq} = J_{wt} + i^2 J_{gen}$, J_{wt} and J_{gen} are wind turbine's rotor and generator inertia, respectively, $\hat{\omega}_r$ is assumed equivalent to ω_g with a notch filter to remove any drive train eigenfrequency component, τ is the time constant of the low pass filter in (3) used to smooth the aerodynamic torque and the filtered output is $\hat{T}_a$. The loss term T_{loss} represents viscous friction, $T_{loss} = b_r\omega_r$, where b_r is the viscocity coefficient. The estimator implementation is shown in Fig. 2.

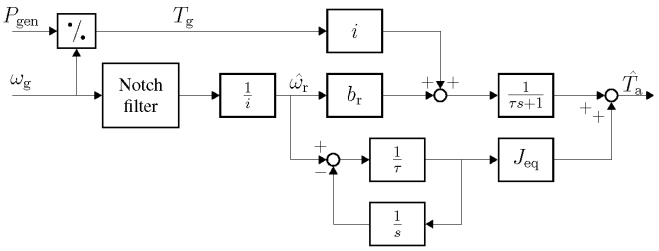

Fig. 2 Block diagram of the estimator implementation with differentiation and low-pass filter.

(1) can be transformed into,

$$\frac{2T_a}{\rho\pi R^5\omega_r^2} = C_p(\lambda)\lambda^{-3}. \tag{4}$$

Based on the estimations of ω_r and T_a, λ is derived by solving (4). Since the real-time calculation of the roots (polynomial equation with high order) is quite time-consuming, the practical implementation might involve a look-up table. The estimated wind speed is decided by $\hat{v} = \frac{\hat{\omega}_r R}{\lambda}$.

By eliminating the speed error between the reference generator speed ω_g^{ref} and the actual generator speed ω_g, the operating point moves to the maximum power point follwing the Optimal Regimes Characteristic (ORC), illustrated in Fig. 3.

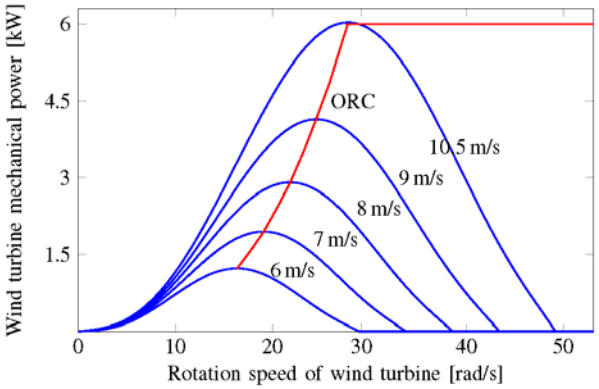

Fig. 3 The ORC curve of the 6kW WECS.

B. Torque Control

As shown in Fig. 1, the wind turbine is coupled to the electrical generator via a gearbox. Thus the rotor speed can be regulated by the generator torque T_g by suitably controlling the AC/DC converter [19].

The widely used vector control structure for the SCIG, based on the rotor fluxorientation, is illustrated in Fig. 4. It is comprised of two decoupled loops. The first is the rotor flux control loop ensuring the field orientation of the induction machine in order to control i_{sd}; the second is a torque control loop which imposes electromagnetic torque to control i_{sq}. The controller will deliver the dq voltage references (u_{sd}^{ref}, u_{sq}^{ref}) and stator flux angle θ_s, which are used to calculate stator voltages (u_{sa}^{ref}, u_{sb}^{ref}, u_{sc}^{ref}).

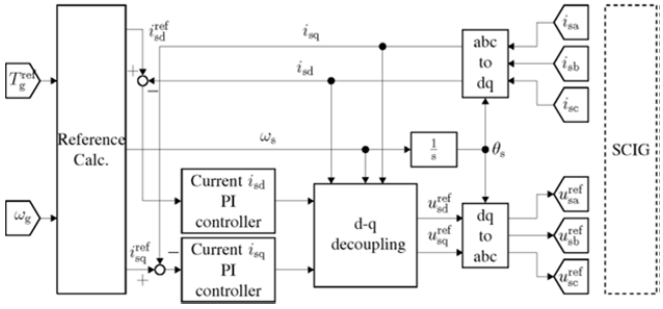

Fig. 4 The Vector Control of a SCIG.

The mathematical derivation of the vector control is well known [31], [32]. The vector control ensures a fast and accurate response. The torque controlled SCIG can be represented by a first-order element with fast dynamics shown in (5). Its time constant τ_G is normally in the milliseconds range.

$$T_g = \frac{1}{1+s\tau_G}T_g^{ref} \tag{5}$$

C. Speed Control

The objective of the speed controller is generating the torque reference T_g^{ref} in order to regulate ω_g by tracking the reference ω_g^{ref}. The wind turbine is described as the following fourth order state space model shown in (6) covering both the flexible drive train and the generator dynamics. The state variables are defined as: $x = [\omega_r, \omega_g, T_{in}, T_g]'$. The input u is T_g^{ref}, u_d is friction torque, ξ is the aerodynamic torque T_a, and the output y is ω_g,

$$\begin{cases} \dot{x}(t) = Ax(t) + B(u(t) + u_d(t)) + E\xi(t) \\ y(t) = Cx(t) \end{cases} \tag{6}$$

with

$$A = \begin{bmatrix} -\frac{b_r}{J_{wt}} & 0 & -\frac{i}{J_{wt}} & 0 \\ 0 & -\frac{b_g}{J_{gen}} & \frac{1}{J_{gen}} & -\frac{1}{J_{gen}} \\ ik_s & -k_s & \frac{b_s i^2}{\eta J_{wt}} + \frac{b_s}{J_{gen}} & \frac{b_s}{J_{gen}} \\ 0 & 0 & 0 & -\frac{1}{\tau_G} \end{bmatrix},$$

$$B = \begin{bmatrix} 0 \\ 0 \\ 0 \\ \frac{1}{\tau_G} \end{bmatrix}, C = \begin{bmatrix} 0 & 1 & 0 & 0 \end{bmatrix}, E = \begin{bmatrix} \frac{1}{J_{wt}} \\ 0 \\ \frac{ib_s}{J_{wt}} \\ 0 \end{bmatrix}.$$

where k_s and b_s are the stiffness and the damping coefficients of the drive train, b_r and b_g are the viscous friction coefficients of the wind turbine rotor and the generator, respectively. They are uncertain but have known upper and lower bounds. The transfer function in the Laplace domain is,

$$y(s) = C(sI - A)^{-1} B(u(s) + u_d(s) + B^{-1} E\xi(s)). \quad (7)$$

Consider u_d and ξ as disturbances, the transfer function takes the following form,

$$y(s) = C(sI - A)^{-1} B(u(s) + d(s)) \quad (8)$$

with $d(s) = u_d(s) + B^{-1} E\xi(s)$.

This model is a strictly proper real (SPR) system with unmodeled disturbances and parameter uncertainties. Normally, a PI controller is designed with closed-loop stability and the dynamic performance around the operating point as satbility and performance requirements. However, with the nonlinear uncertainty due to the movement of the operating points and disturbances, adequate transient performance cannot be guaranteed using a PI controller. Therefore, an $\mathcal{L}_1$ adaptive controller is employed to handle these problems.

III. Design of the $\mathcal{L}_1$ Adaptive Controller

A. Problem Formulation

For the WECS represented by the Single Input and Single Output (SISO) system (Section II-C), the $\mathcal{L}_1$ adaptive output feedback controller can be designed to ensure uniformly bounded transient response for both input and output. These are inherent features of this control architecture [26]-[28]. The control objective here is to enable the system output ω_g to follow the reference ω_g^{ref}. Since the first-order reference system has good dynamic performance, the reference transfer function model $M(s)$ with time constant τ_m is,

$$M(s) = \frac{1}{s\tau_m + 1} = \frac{m}{s+m}, \quad \tau_m = \frac{1}{m}, \quad m > 0. \quad (9)$$

Consider the following system,

$$y(s) = A(s)(u(s) + d(s)), \quad (10)$$

where $u(s)$ is the Laplace transform of the system input $T_g^{ref}(s)$, $y(s)$ is $\omega_g(s)$, $A(s)$ represents the strictly proper unknown transfer function of the the WECS, $d(s)$ represents nonlinear uncertainties and disturbance, denoted by $d(t) = f(t, y(t))$.

For the $f(t, y(t))$, two assumptions are made.

Assumption 1: (Lipschitz condition) There exist constants $L > 0$ (Lipschitz gain) and $L_0 > 0$, possibly arbitrarily large, such that the following inequalities hold uniformly:

$$\begin{cases} |f(t, y_1) - f(t, y_2)| \le L|y_1 - y_2| \\ |f(t, y)| \le L|y| + L_0, \quad L > 0, L_0 > 0. \end{cases} \quad (11)$$

Assumption 2: The variation rate of uncertainties is uniformly bounded: there exist three constants $L_1, L_2, L_3 > 0$, such that, for $t \ge 0$,

$$|\dot{d}(t)| \le L|y_1 - y_2| \le L_1|\dot{y}(t)| + L_2|y(t)| + L_3 \quad (12)$$

Based on (9) and (10), the system can be rewritten in terms of the reference model as,

$$y(s) = M(s)(u(s) + \sigma(s)) \quad (13)$$

where,

$$\sigma(s) = \frac{(A(s) - M(s))u(s) + A(s)d(s)}{M(s)}. \quad (14)$$

B. Structure of the $\mathcal{L}_1$ Adaptive Controller

A typical closed loop $\mathcal{L}_1$ adaptive controller is illustrated in Fig. 5. It consists of a state predictor, the adaptation law and the control law.

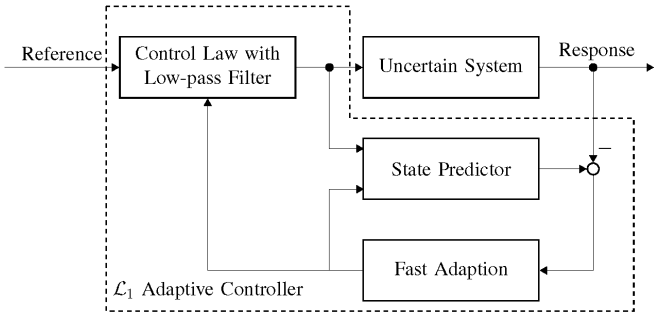

Fig. 5 A typical closed loop $\mathcal{L}_1$ adaptive controller [25].

1) State (Output) predictor:

$$\dot{\hat{y}}(t) = -m\hat{y}(t) + m(u(t) + \hat{\sigma}(t)), \quad \hat{y}(0) = 0 \quad (15)$$

where $\hat{\sigma}(t)$ is the adaptive estimate.

2) Adaptation law: The adaptation of $\hat{\sigma}(t)$ is defined as,

$$\dot{\hat{\sigma}}(t) = \Gamma \mathrm{Proj}(\hat{\sigma}(t), -\tilde{y}(t)) \quad \hat{\sigma}(0) = 0 \quad (16)$$

where $\tilde{y}(t) = \hat{y}(t) - y(t)$ is the error signal between the output and the predictor, and Γ is the adaptation gain. Projection methods are introduced to ensure the boundary of the parameter estimation. The projection is bounded by,

$$\hat{\sigma}(t) \le \Delta, \quad (17)$$

where Δ is the boundary.

The adaptive system tracks the state predictor, while the state predictor matches the expected closed loop reference system output very closely. The tracking errors of these signals go to zero as the adaptation gain $\Gamma \to \infty$.

3) Control law with low-pass filter: This block is used to compensate the uncertainties only within a desired bandwidth,

$$u(s) = C(s)(r(s) - \hat{\sigma}(s)) \quad (18)$$

where $r(s)$ is the reference signal which $y(s)$ should follow and $C(s)$ is the low pass filter with cutoff angular frequency w and $C(0) = 1$. The DC gain of one ensures reference

tracking. Because of the approximation of $\hat{\sigma}$, the low pass filter $C(s)$ is used to prevent high frequency chatter from passing into the system.

$$C(s) = \frac{w}{s+w}. \tag{19}$$

C. Closed Loop Reference System

Following [25], suppose the adaptive variable $\hat{\sigma}$ was exactly estimated, $\hat{\sigma} = \sigma$, the closed loop reference system would be given by,

$$y_{\text{ref}}(s) = M(s)(u_{\text{ref}}(s) + \sigma_{\text{ref}}(s)), \tag{20}$$

$$u_{\text{ref}}(s) = C(s)(r(s) - \sigma_{\text{ref}}(s)), \text{ and} \tag{21}$$

$$\sigma_{\text{ref}}(s) = \frac{(A(s) - M(s))u_{\text{ref}}(s) + A(s)d_{\text{ref}}(s)}{M(s)}. \tag{22}$$

Substituting (19) and (20) into (18):

$$y_{\text{ref}}(s) = (C(s)r(s) + (1 - C(s))d_{\text{ref}}(s)). \tag{23}$$

The closed loop reference to output transfer function is,

$$H(s) = \frac{A(s)M(s)}{C(s)A(s) + (1 - C(s))M(s)}. \tag{24}$$

Thus $M(s)$ and $C(s)$ should be chosen to ensure that $H(s)$ is stable. The following lemma from [25] is used in the design.

Lemma: (Cao and Hovakimyan) Let $C(s)$ and $M(s)$ verify the $\mathcal{L}_1$-norm condition (25), then the closed loop reference function ((20) to (22)) is Bounded Input and Bounded Output (BIBO) stable.

$$\|G(s)\|_{L_1} L < 1 \tag{25}$$

where $G(s) = H(s)(1 - C(s))$.

Similarly, substituting u_{ref} from (21) into (22), the following closed loop function can be derived,

$$\sigma_{\text{ref}}(s) = \frac{C(s)(A(s) - M(s))r_{\text{ref}}(s) + A(s)d_{\text{ref}}(s)}{C(s)A(s) + (1 - C(s))M(s)}, \tag{26}$$

which has the same denominator $H(s)$. Hence σ_{ref} is stable if $H(s)$ is stable.

D. Determination of the controller parameters

The approximation of the system $A(s)$ is used in the analysis and it is expected that small variations of $A(s)$ will not change the properties of the control method. As described in Section C, $A(s)$ can be defined as the following transfer function of the 6 kW variable speed WECS [21] in this study according to (7). The parameters of the 6 kW variable speed WECS are listed in the Appendix.

$$A(s) = \frac{A_n(s)}{A_d(s)} = C(sI - A)^{-1}B \tag{27}$$

Accordingly, the closed loop reference transfer function is,

$$H(s) = \frac{m\ (s+w)A_n(s)}{w\ (s+m)A_n(s) + m\ s\ A_d(s)}. \tag{28}$$

In order to get faster response, let the closed loop reference time constant $\tau_m = 0.1\text{s}$, therefore $m = 10$ [rad/s]. To ensure $H(s)$ is stable, its poles must be in the left half of the complex plane which restricts the choices of $M(s)$ and $C(s)$. Instead of solving a polynomial equation, one possible method of checking the stability of $H(s)$ is by using the root locus method, shown in Fig. 6 (a). The poles are always located in the left half complex plane if $w > 0$.

From (24), it is obvious that if the cutoff frequency of the lowpass filter $C(s)$ is very high, $C(s)$ is like an all-pass filter and $C(s) \approx 1$. It draws $H(s) \approx M(s)$, which means the system responses are same as the reference model. Therefore, increasing the cutoff frequency of the low-pass filter can lead to a better match. However, a low-pass filter with high cutoff frequency may result in high gain feedback and thus lead to a closed-loop system with a small robustness margin and too high amplification of measurement noises. As a balance, $w = 30$ is used here.

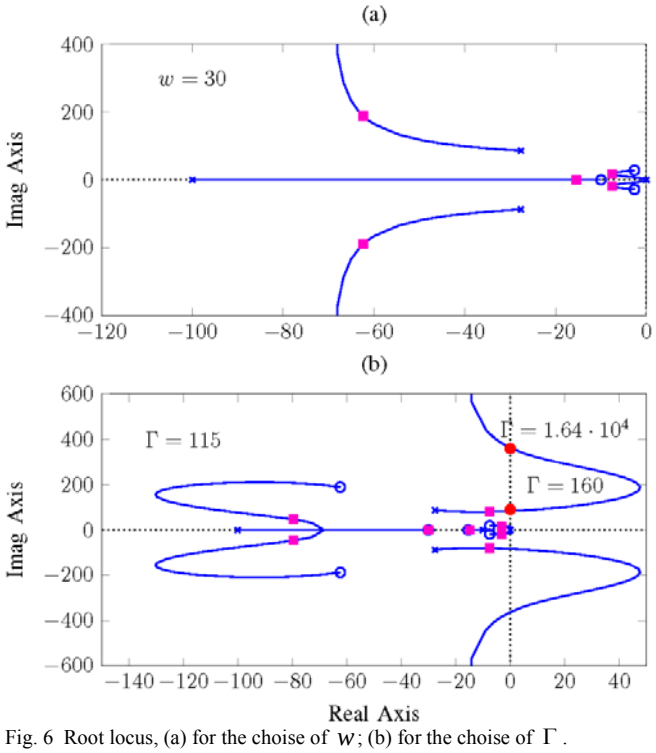

Fig. 6 Root locus, (a) for the choise of w; (b) for the choise of Γ.

Assuming that the estimator $\hat{\sigma}(s)$ in (20) does not reach the boundary,

$$\dot{\hat{\sigma}}(t) = \Gamma(y(t) - \hat{y}(t)) \tag{29}$$

leading to the following closed-loop system,

$$\hat{\sigma}(s) = \frac{C(s)(A(s) - M(s))r(s) + A(s)d(s)}{\frac{1}{\Gamma}s + C(s)A(s) + (1 - C(s))M(s)}. \tag{30}$$

Obviously, the stability of the estimator $\hat{\sigma}(s)$ depends on Γ and its value range can be obtained by performing a root locus of the transfer function $J(s)S(s)$, where

$$J(s) = C(s)A(s) + (1 - C(s))M(s) \tag{31}$$

$$S(s) = \frac{1}{s} \tag{32}$$

According to the root locus of the adaptation gain Γ, shown in Fig. 6 (b), Γ should fulfill $\Gamma < 160$ or $\Gamma > 1.64 \times 10^4$. To obtain an adequate stability margin, $\Gamma = 115$ is chosen.

IV. Simulation and Results

In order to verify the developed $\mathcal{L}_1$ adaptive controller for the MPPT of WECSs, several case studies were carried out, which includes step responses, validation of the wind speed estimation and the tracking performance under wind speed variations. The optimal values of the tip speed ratio and the power coefficient are $\lambda_{opt} = 7$ and $C_p^{max} = 0.4763$.

A. Step response

The $\mathcal{L}_1$ adaptive controller is tested under different step changes of wind speed. This simulation shows the effects of a sudden change of aerodynamic torque T_a, similar to wind shear and tower shadow effects in real operation. The step responses of λ and C_p are shown in Fig. 7. Due to the step change of the wind speed, there is a sudden change of λ, and C_p drops accordingly. Then the λ is regulated to return to its optimal value λ_{opt} quite fast (less than 0.5 s) even for large step changes (from 7 m/s to 10 m/s). The wind turbine recovers to track the maximum power point.

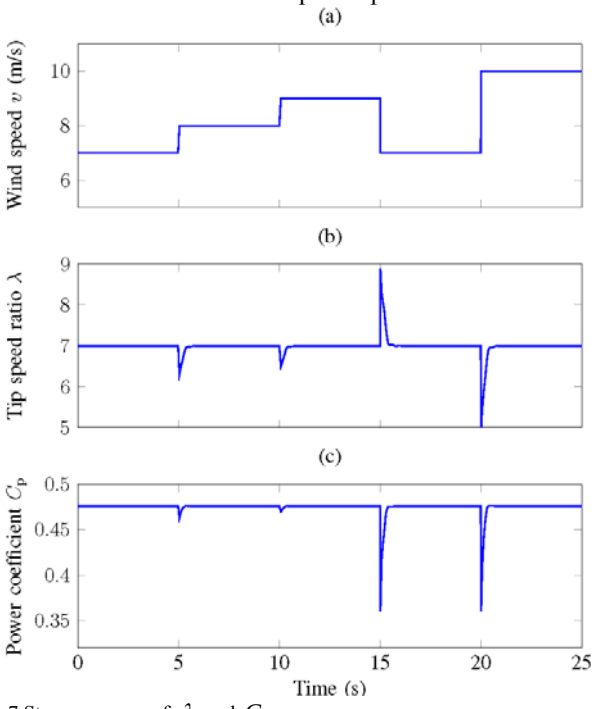

Fig. 7 Step responses of λ and C_p.

B. Validation of wind speed estimation

The accuracy of the wind speed estimation is tested as well.

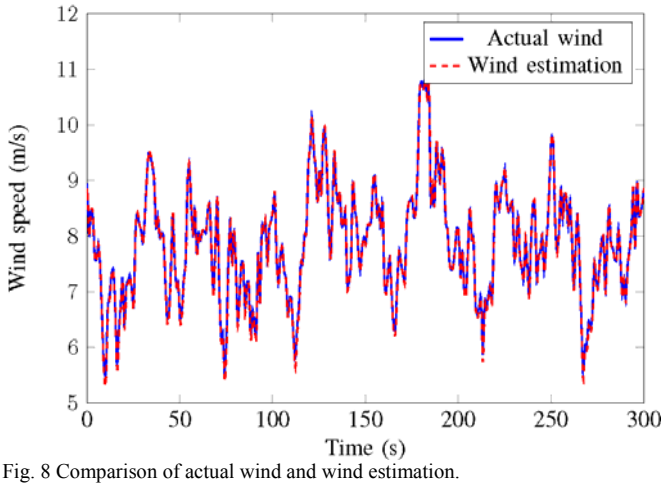

Fig. 8 Comparison of actual wind and wind estimation.

In this case study, the wind profile applied has been derived by using the Von Karman spectrum in the IEC standard, with an average wind speed of 7 m/s and a median turbulence intensity of 0.15. The variation covers most of the range of normal wind speed-between 5 m/s and 11 m/s. The simulation time is 300 s. The wind speed is estimated by means of the method described in Section II-A. The comparison between the actual and the estimated wind speed is shown in Fig. 8. It can be observed that the two curves are in good agreement. The standard deviation is 0.0657 m/s.

C. Tracking performance with wind speed variation

Since the accuracy of the wind speed estimation is satisfactory, the tracking performance of the speed reference ω_g^{ref} is the key factor to determine the power efficiency and production. This case study is divided into two scenarios based on the different turbulence intensities of wind profiles: Scenario 1 and Scenario 2, shown in Fig. 9 (a). The time-varying viscous coefficients (b_r , b_g) and the other disturbances except the viscous friction are randomly generated within bounds, as shown in Fig. 9 (b) and (c). The simulation time is 300 s.

As mentioned in Section II-C, a PI controller is normally used based on the same SISO WECS considering the closed-loop stability and transient performances. The PI controller can stabilize the system in the presence of the unmodeled dynamics and disturbances $d(t)$. However, the transient performance of tracking the reference signal is sacrificed.

The tracking performances of the $\mathcal{L}_1$ adaptive controller and the PI controller are illustrated in Fig. 10-13.

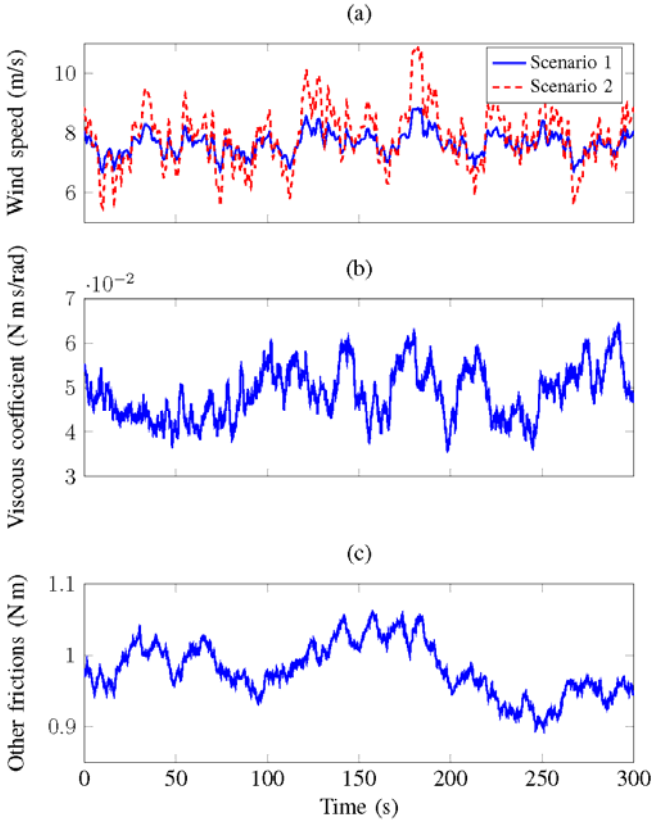

Fig. 9. Friction disturbances.

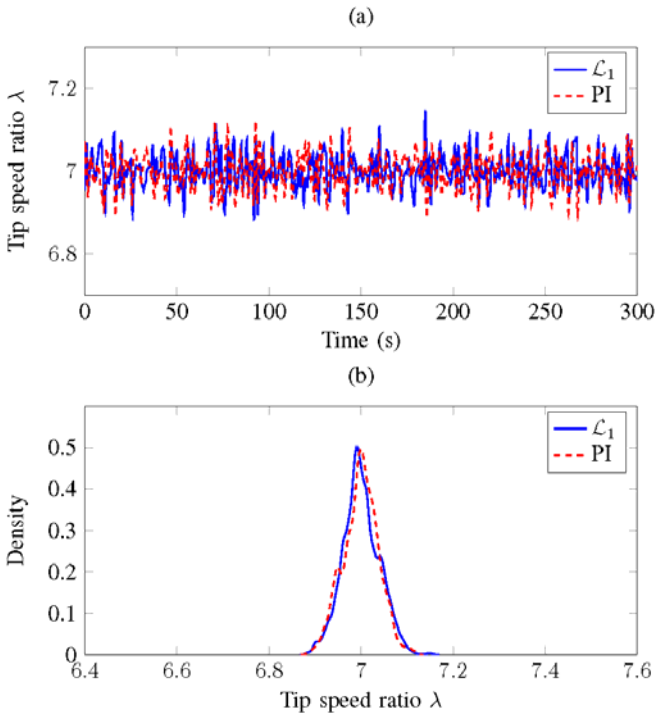

Fig. 10 Comparison of λ variation during the operation in Scenario 1: (a) in time series format; (b) λ in density format.

For Scenario 1, since the turbulence intensity is small, the wind speed is limited between 7 m/s and 8.5 m/s. Both controllers show good capability in keeping the wind turbine operating around λ_{opt} during simulation, between 6.85 and 7.15 . From the density point of view (Fig. 10), it is much clearer that both controllers have similar tracking performances in the presence of disturbances and parameter uncertainties. Accordingly, the energy efficiency is maintained at a high level ($0.4755 \sim 0.4763$) shown in Fig. 11. The power production, which is almost the same for both controllers, is shown in Table I. The energy captured with the $\mathcal{L}_1$ controller is 0.02% higher.

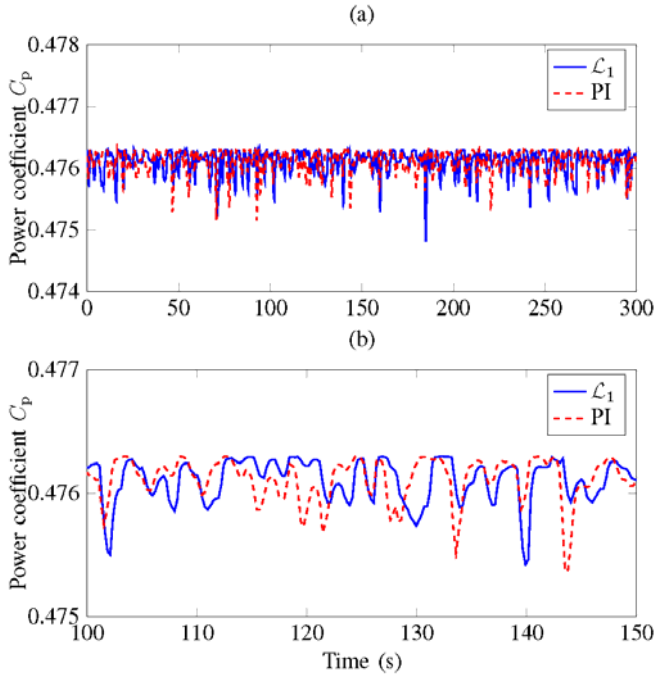

Fig. 11 Efficiency comparison during the operation in Scenario 1. (a) Full time frame; (b) Zoomed in time frame ($100\text{s} \sim 150\text{s}$).

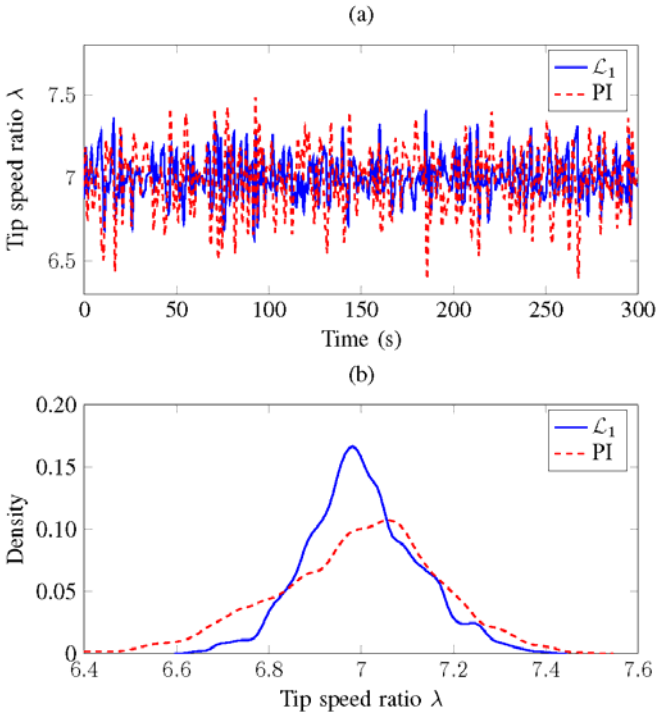

Fig. 12. Comparison of λ variation during the operation in Scenario 2: (a) in time series format; (b) λ in density format.

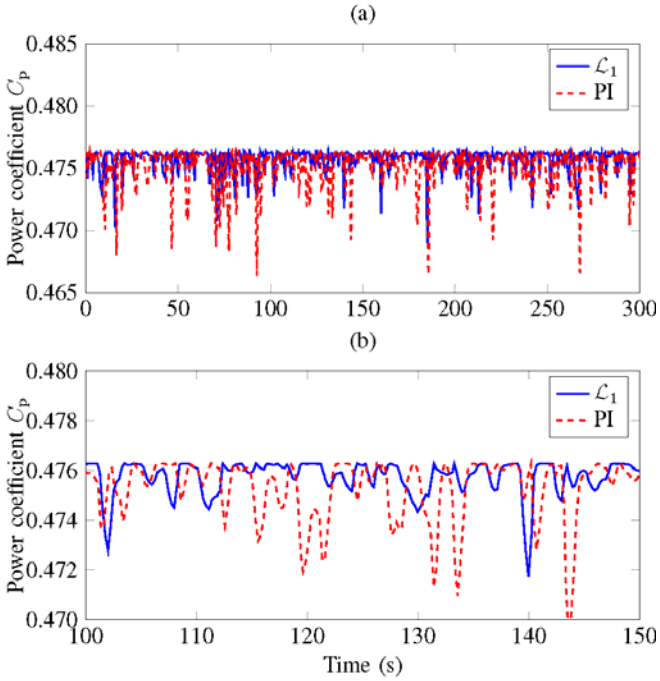

Fig. 13 Efficiency comparison during the operation in Scenario 2. (a) Full time frame; (b) Zoomed in time frame (100s $\sim$ 150s).

For Scenario 2, the turbulence intensity is larger and the wind speed variation is expanded between 5.5 m/s and 10.5 m/s, thereby covering all partial load regimes. The tracking performances of both controllers are influenced and become worse compared with Scenario 1. As illustrated in Fig. 12, the $\mathcal{L}_1$ adaptive controller shows better capability of keeping the wind turbine operating at its optimal tip speed ratio λ_{opt} than the PI controller. The tip speed ratios with the $\mathcal{L}_1$ controller are distributed between 6.8 and 7.2 while those with the PI controller are distributed between 6.6 and 7.4 . Without precise tracking, the energy efficiency of the wind turbine by using the PI control is lower, as shown in Fig. 13. The power production for both controllers are listed in Table I. The energy captured with the $\mathcal{L}_1$ controller is 0.59% higher in Scenario 2 than that of the PI controller.

TABLE I
ENERGY PRODUCTION COMPARISON

Controller	Energy production (Scenario 1)	Energy production (Scenario 2)
PI	432409.50 J	526661.51 J
$\mathcal{L}_1$	432510.05 J	529787.99 J
Benefit of $\mathcal{L}_1$ (absolute)	100.55 J	3126.48 J
Benefit of $\mathcal{L}_1$ (percent)	0.02%	0.59%

V. CONCLUSION

With WECSs being nonlinear systems with significant parameter uncertainties, in particular friction coefficients, and subject to disturbances, in the form of nonlinear and unmodeled aerodynamics, the $\mathcal{L}_1$ adaptive speed control proposed this paper avoided the accurate WECS modeling. Instead, the WECS was modeled as a transfer function with the generator torque as the input and the generation speed as the output . Based on this simplified model, an $\mathcal{L}_1$ adaptive speed controller was designed in order to achieve a tradeoff between the transient performance and the stability of the MPPT under disturbances. The $\mathcal{L}_1$ adaptive speed controller showed good trackingperformance towards the optimum tip speed ratio and robustness with fast adaptation to uncertainties and disturbances as shown in detailed simulation cases that included wind shear, shadow effects and wind speed variations. Compared with the converntional optimized PI controller, the proposed $\mathcal{L}_1$ adaptive speed control for MPPT captures more energy during operation, especially in highly turbulent wind conditions. Therefore, The proposed $\mathcal{L}_1$ adaptive control is a reasonable alternative to the PI control and may present some advantages for MPPT in highly turbulent wind conditions.

APPENDIX

The 6 kW variable-speed-fixed pitch WECS, introduced in [19], is used in the test case. The parameters of the WECS are listed in Table II.

TABLE II
PARAMETER FOR LOW POWER (6 KW) WECS

Symbol	Description	value	Part
R	Blade length	2.5 m	Turbine rotor
i	Multiplier ratio	6.25	Drive train
J_{wt}	Rotor inertia	3.6 kg $\cdot$ m^2	Drive train
J_{g}	Generator inertia	0.01 kg $\cdot$ m^2	Drive train
η	Efficiency	0.95	Drive train
k_{s}	Stiffness	75 N $\cdot$ m/rad	Drive train
b_{s}	Damping	0.5 kg $\cdot$ m^2/s	Drive train
p	Pole pair	2	SCIG
R_{s}	Stator resistance	1.265 Ω	SCIG
R_{r}	Rotor resistance	1.43 mΩ	SCIG
L_{m}	Mutual reactance	0.1397 H	SCIG
L_{s}	Stator reactance	0.1452 H	SCIG
L_{r}	Rotor reactance	0.1452 H	SCIG
w_{s}	Synchronous speed	100π rad/s	SCIG
U_{s}	Voltage level	220 V	SCIG

ACKNOWLEDGEMENT

The authors thank the Sino-Danish Center for Education and Research (SDC) for the financial support to the PhD project of “Coordinated Control of Wind Power Plants and Energy Storage Systems.” The authors would also like to thank Robin Broder Hytowitz, a PhD student from Johns Hopkins University and a visiting scholar with Centre for Electric Power and Energy (CEE), Department of Electrical Engineering, Technical University of Denmark (DTU), for proofreading the paper.

REFERENCES

[1] V. Fthenakis and H. C. Kim, "Land use and electricity generation: A life-cycle analysis," *Renewable and Sustainable Energy Reviews*, vol. 13, pp. 1465 – 1474, 2009.

[2] REN21, "Renewables 2011: Global status report," REN21, Tech. Rep., 2011.

[3] P. Sørensen, A. D. Hansen K. Thomasen, T. Buhl, P. E. Morthorst, L. H. Nielsen, F. Lov, F. Blaabjerg, H. A. Nielsen, H. Madsen and M. H. Donovan, "Operation and control of large wind turbines and wind farms," Risø National Laboratory, Roskilde, Denmark, Tech. Rep. Risø-R 1532, Sep. 2005.

[4] R. Carriveau, Fundamental and Advanced Topics in Wind Power. InTech, 2011.

[5] Z. Chen, J. M. Guerrero, and F. Blaabjerg, "A review of the state of the art of power electronics for wind turbines," *IEEE Trans. Power Electron.*, vol. 24, no. 8, pp. 1859-1875, 2009.

[6] E. Koutroulis and K. Kalatizakis, "Design of a maximum power point tracking system for wind energy conversion applications," *IEEE Trans. Ind. Electron.,* vol. 53, no. 2, pp. 486-494, 2006.

[7] Z. M. Dalala, Z. U. Zahid, and J.-S. Lai, "New overall control strategy for small-scale WECS in MPPT and stall regions with mode transfer control," *IEEE Trans. Energy Convers.,* vol. 28, no. 4, pp. 1082-1092, 2013.

[8] R. Datta and V. Ranganathan, "A method of tracking the peak power points for a variable speed wind energy conversion system," *IEEE Trans. Energy Convers.*, vol. 18, no. 1, pp. 163–168, 2003.

[9] Q. Wang and L. Chang, "An intelligent maximum power extraction algorithm for inverter-based variable speed wind turbine systems," *IEEE Trans. Power Electron.*, vol. 19, no. 5, pp. 1242 – 1249, 2004.

[10] Z. M. Dalala, Z. U. Zahid, W. Yu, Y. Cho, and J. S. Lai, "Design and analysis of an MPPT technique for small-scale wind energy conversion systems," *IEEE Trans. Energy Convers.*, vol. 28, no. 3, pp.756–767, 2013.

[11] S. M. Barakati, M. Kazerani, and J. D. Aplevich, "Maximum power tracking control for a wind turbine system including a matrix converter," *IEEE Trans. Energy Convers.*, vol. 24, no. 3, pp. 705-713, 2009.

[12] K.-H. Kim, T. L. Van, D.-C. Lee, S.-H. Song, and E. -H. Kim, "Maximum output power tracking control in variable-speed wind turbine systems considering rotor inertial power," *IEEE Trans. Ind. Electron.*, vol. 60, no. 8, pp. 3207–3217, 2013.

[13] C.-T. Pan and Y.-L. Juan, "A novel sensorless MPPT controller for a high-efficiency microscale wind power generation system," *IEEE Trans. Energy Convers.,* vol. 25, no. 1, pp. 207–216, 2010.

[14] A. Abo-Khalil and D.-C. Lee, "MPPT control of wind generation systems based on estimated wind speed using SVR," *IEEE Trans. Ind. Electron.*, vol. 55, no. 3, pp. 1489–1490, 2008.

[15] H. Li, K. Shi, and P. McLaren, "Neural-network-based sensorless maximum wind energy capture with compensated power coefficient," *IEEE Trans. Ind. Appl.*, vol. 41, no. 6, pp. 1548–1556, 2005.

[16] W. Qiao, X. Yang, and X. Gong, "Wind speed and rotor position sensorless control for direct-drive PMG wind turbines," *IEEE Trans. Ind. Appl.*, vol. 48, no. 1, pp. 3–11, 2012.

[17] S. Bhowmik, R. Spee, and J. H. Enslin, "Performance optimization for doubly fed wind power generation systems," *IEEE Trans. Ind. Appl.*, vol. 35, no. 4, pp. 949–958, 1999.

[18] M. N. Soltani, T. Knudsen, M. Svenstrup, R. Wisniewski, P. Brath, R. Ortega, and K. Johnson, "Estimation of rotor effective wind speed: A comparison," *IEEE Trans. Control Syst. Technol.*, vol. 21, no. 4, pp. 1155–1167, 2013.

[19] I. Munteanu, A. Bractu, N. A. Cutululis and E. Ceangă, *Optimal control of wind energy systems- Towards a Global Approach*. Springer, 2008.

[20] I. Munteanu, S. Bacha, A. Bratcu, J. Guiraud, and D. Roye, "Energy-reliability optimization of wind energy conversion systems by sliding mode control," *IEEE Trans. Energy Convers.*, vol. 23, no. 3, pp. 975 – 985, Sep. 2008.

[21] B. Beltran, M. Benbouzid, and T. Ahmed-Ali, "Second-order sliding mode control of a doubly fed induction generator driven wind turbine," *IEEE Trans. Energy Convers.*, vol. 27, no. 2, pp. 261–269, 2012.

[22] J. Mauricio, A. Leon, A. Gomez-Exposito, and J. Solsona, "An adaptive nonlinear controller for DFIM-based wind energy conversion systems," *IEEE Trans. Energy Convers.*, vol. 23, no. 4, pp. 1025 –1035, Dec. 2008.

[23] M. G. Simoes, B. K. Bose, and R. J. Spiegel, "Fuzzy logic based intelligent control of a variable speed cage machine wind generation system," *IEEE Trans. Power Electron.*, vol. 12, no. 1, pp. 87–95, 1997.

[24] V. Galdi, A. Piccolo, and P. Siano, "Designing an adaptive fuzzy controller for maximum wind energy extraction," *IEEE Trans. Energy Convers.,* vol. 23, no. 2, pp. 559–569, 2008.

[25] C. Cao and N. Hovakimyan, $\mathcal{L}_1$ *Adaptive Control Theory, Guaranteed Robustness with Fast Adaptation*. SIAM, 2010.

[26] C. Cao and N. Hovakimyan, "Design and analysis of a novel $\mathcal{L}_1$ adaptive control architecture with guaranteed transient performance," *IEEE Trans. Autom. Control*, vol.53 no.2 pp 586-591, 2008.

[27] C. Cao and N. Hovakimyan, "Stability margins of $\mathcal{L}_1$ adaptive control architecture," *IEEE Trans. Autom. Control*, vol 55 no.2, pp 480-487, 2010.

[28] K-K Kim and N. Hovakimyan, "Multi-Criteria Optimization for Filter Design of $\mathcal{L}_1$ Adaptive Control," *Journal of Optimization Theory and Applications*, 2014.

[29] E. Kharisov, N. Hovakimyan and K. J. Åström, "Comparison of architectures and robustness of model reference adaptive controllers and $\mathcal{L}_1$ adaptive controllers" *Int. Journal of Adaptive Control and Signal Processing*. 2014.

[30] H. Geng, G. Yang, D. Xu, and B. Wu, "Unified power control for PMSG-based WECS operating under different grid conditions," *IEEE Trans. Energy Convers.*, vol. 26, no. 3, pp. 822 –830, Sep. 2011.

[31] B. K. Bose, *Modern power electronics and AC drives*. Prentice-Hall, 2001.

[32] W. Leonhard, *Control of electrical drives*. Springer, 2001.